ESTIMATION OF RADIOMETRIC PERFORMANCE OF ELECTRO-OPTICAL IMAGING SENSOR OF LOW EARTH EQUATORIAL ORBIT LAPAN SATELLITE

Ahmad Maryanto[1]*, Andy Indradjad[1], Dinari Nikken Sulastrie Sirin[1], and Ayom Widipaminto[1]
[1]Indonesian National Institute of Aeronautics and Space (LAPAN)
*e-mail: a_maryanto@yahoo.com

Abstract. Study of spectro-radiometric performance of electro-optical imager which is planned to be launched on low earth equatorial orbit LAPAN satellite was conducted through simulative calculation of image irradiance and its associated generated voltage at the image detector output. Simulative calculation was applied to three scenarios of selected spectral bands. Those spectral bands were selected spectra (1), which consisted of spectral bands B = (390-540 and 790-900) nm, G = (470-610 and 700-900) nm, and R = (590-650 and 650-900) nm; selected spectra (2) consisted of B1 = (390-540) nm, G1 = (470-610) nm, and R1 = (590-650) nm; and selected spectra (3) consisted of B1(Green) = (525-605) nm, B2(Red) = (630-690) nm, and B3(NIR) = (750-900) nm, on three scenarios of optical aperture or f-number (N) 2.8, 4.0, and 5.6. Green grasses, dry grasses, and conifers were examples of the imaged target, chosen as representation of vegetations. Kodak KLI-8023 was used as the optical detector. The integration time was assumed 3 miliseconds which correspond to about 20 m ground sampling distance (GSD). Solar zenith angle were varying from 90° (early morning) to 0° (solar noon). The results showed that option (3) of selected spectra, as proposed for pushbroom imager of LAPAN satellite, was relatively accepted to be implemented and complemented with f-number 4.0 of optical system used. Whereas simulation RGB color displayed composed by R = B2(Red), G = B3(NIR), B = B1(Green) also showed a greenish color sense as expected for vegetation imaged target.

Keywords: *image irradiance, solar zenith angle, imager LAPAN satellite*

1 INTRODUCTION

Understanding measured radiant energy recorded by detecting device of imaging sensor is one of the most impotant issues in low earth equatorial orbit remote sensing satellites. Radiant energi collected at the detection plane is a product of radiant flux density at image plane (image irradiance) and duration time in which radiant flux density is accounted (how long the optical detector being exposed). As satellite travels along equator (or near equator) line, low earth equatorial orbit remote sensing satellites will capture imaged target (earth surface) at very wide variation of sun irradiation level, from extreme dark (no sun irradiation at early morning) to extreme bright (highest sun irradiation at noon). For a 12 minutes pass, the satellite will span 3 time zones which mean that in a single image, the local time in one edge of this image will be 3 hours less than the local time in the other edge, causing great change in the irradiation level and the size of the shadows. Besides that fact, the satellite will pass over a region several times during the day, during the morning, noon, and in the afternoon. This problem, of course, will cause some difficulties and challenges either for the applicants (end users) or the system designer.

Having succeeded with low sun-synchronous orbit micro satellite, LAPAN will continue its satellite-technology mastery program by developing the next satellite that are named LAPAN A2, LAPAN A3 and so on. LAPAN A2 and/or LAPAN A3 are experimental satellites of the same class with LAPAN A1 but with some changes in development methodology and its payload. LAPAN A2 and LAPAN A3 will be fully assembled, integrated and tested (AIT) in Indonesia. A2/A3 satellite will carry pushbroom imaging sensor as the predecessor of remote sensing satellite technology development in Indonesia. Moreover, one of these satellites will be placed in equatorial orbit (NEqO) to explore the advantages and disadvantages of it for remote sensing (Hasbi *et al.*, 2010).

The idea of using low earth equatorial orbit as an alternative orbit for remote sensing satellite was proposed long time ago. Salatun *et al.* (1975) discussed various considerations regarding the typical of orbit satellites for remote sensing in Indonesia. Tropical Earth Resources Satellite (TERS) Program was one of the equatorial orbit

utilization initiators for remote sensing in Indonesia (Hoeke and Linsen, 1984). Brazil with the SSR idea proposed utilization plan of the low equatorial orbit on 1995, while Malaysia with Razaksat program also put forward ideas the use of NeqO low-orbit for their satellites. Nevertheless, only few countries or space agencies implemented NeqO low-orbit, such as Malaysia with Razaksat-1 satellite which was launched on July 14, 2009. Unfortunately, the availability of publication about data, processing and utilization of the data, and the technical aspects of the design of optical imaging systems for the orbit is still limited.

This paper discusses about LAPAN satellite imager, focusing on its radiometric performance estimation by numerically simulation. Simulation calculated the radiant flux density formed at the image plane (image irradiance). Then, associated it with the light response characteristics and charge well capacities of Kodak KLI-8023 CCD as a detection device that will be used in LAPAN imager. Calculation was applied to the 3 schemes spectral bands with 3 schemes of optical system aperture or f-number (N). The imaged target was green grasses. This estimation was expected to be one of the recommendations input to speed up the iteration process in designing imaging sensor system for low earth equatorial orbit LAPAN satellite. The three spectral band schemes referred to in this work are listed in Table 1, whereas the three schemes for f-number (N) are N = 2.8, N = 4.0, and N = 5.6.

2 IMAGE IRRADIANCE IN IMAGING REMOTE SENSING

2.1 Camera Equation

Suppose an arrangement of extended object, optical system, and image plane as shown in Figure 1, it is assumed that the entrance pupil diameter of optical system is D, object radiance is L_o equal in all direction (object is lambertian/perfectly diffuse reflector), the second focal distance of optical system is f', θ_m is angle of marginal ray in object space, and θ'_m is angle of marginal ray in image space. For an on-axis elemental area of object dA_o, the total radiant flux intercepted by entrance pupil $d\Phi_o$, is given by Slater (1980):

$$d\Phi_o = \pi L_o dA_o sin^2\theta_m \quad (1)$$

where $\pi sin^2\theta_m = \Omega$ is solid angle of light cone formed by entrance pupil with apex angle $2\theta_m$ in object space.

By optical system, those radiant flux will be transferred to image space, leaving the exit pupil and forming an image cone with apex angle $2\theta'_m$ in the image direction, and give rise an image radiance L_i at an elemental area dA_i at the image plane.

Table 1. THREE SPECTRAL BAND SCHEMES

Spectral band scheme	Band-1 (nm)	Band-2 (nm)	Band-3 (nm)
Same as KLI-8023	B: 390-540 and 790-900	G: 470-610 and 700-900	R: 590-650 and 650-900
KLI-8023 plus additional filter	B1: 390-540	G1: 470-610	R1: 590-650
Same as DMC or ETM+/LS-7 (band 2,3,4)	B1 (Green): 525-605	B2 (Red): 630-690	B3(NIR): 750-900

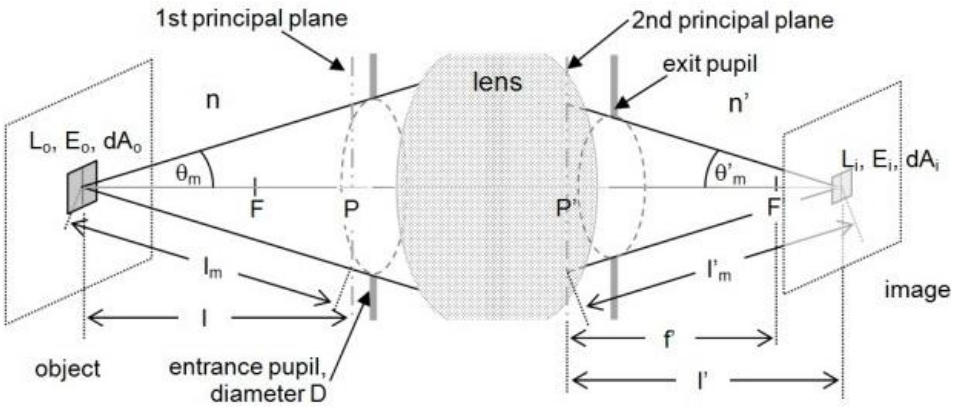

Figure 1.Imaging geometry in an optical system (camera), showing several important quantities involved in the radiant energy transfer from object to image plane

Using the similar reasoning as in object space, we may express the radiant flux at image plane as:

$$d\Phi_i = \pi L_i dA_i sin^2\theta'_m \quad (2)$$

In a lossless system, $d\Phi_i = d\Phi_o$, and therefore:

$$\pi L_o dA_o sin^2\theta_m = \pi L_i dA_i sin^2\theta'_m \quad (3)$$

as $(dA_o/dA_i) = M^2$, and the Abbe sine condition is hold in the optical system used, therefore, $(\sin\theta'_m/\sin\theta_m) = (n/n')M$ where n = n' = 1 (the refraction indices for object space and image space), from equation (3) it is clear that in a lossless system:

$$L_o = L_i \quad (4)$$

as $(d\Phi_i/dA_i)$ is the image flux density (image irradiance) E_i, from equation (2) and equation (4) we get:

$$E_i = \pi L_o sin^2\theta'_m \quad (5)$$

For imaging of a distant object as in satellite remote sensing, second principal plane of optical system is no longer flat but a spherical surface centered at second focal point F' with radius f' (see Figure1) which means $l'_m = f'$, and therefore:

$$sin\theta'_m = \frac{D}{2f'} = \frac{1}{2N} \quad (6)$$

where (f'/D) = N is the focal number (f-number) of the optical system. Therefore, equation (5) can be rewritten as:

$$E_i = \pi L_o/4N^2 \quad (7)$$

Equation (7) or the similar is called camera equation which is describing radiant energy transfer from object to image for an on-axis imagery of a distant object.

For an object on a certain distance, the general form of camera equation is given by Slater (1980), Holst (2007), Nakamura (2006), and Lee (2005):

$$E_i = \frac{\pi L_o}{4N^2(1-M)^2} \quad (8)$$

where M is lateral magnification.

In a real system, image irradiance calculation has to include into account several factors that can affect the total radiant energy collected at the image plane, i.e. Slater (1980):

- Losses due to reflection, absorption, and scattering that can be lumped together in the factor τ_o (optical transmission)
- Losses with a factor $1-A^2$ due to the presence of central obscuration (such as occurred in a cassegrainian system), where A is the ratio of central obscuration diameter to that of the primary mirror
- Reduction by factor $\cos^n\alpha$ due to decreasing image forming cone and increasing obliquity for off axis images, where n = 4 (for simple lens), and α is the angle between optical axis and chief ray of the off axis image.
- Progresif reduction with factor $K_N(\alpha)$ due to vignetting.

Therefore, general form of camera equation can be rewritten as:

$$E_i = \frac{\pi(1-A^2)K_N(\alpha)cos^n\alpha L_o\tau_o}{4N^2(1-M)^2} \quad (9)$$

2.2 Image Irradiance at the Remote Sensing Imagery

For a perfectly difuse reflector, as assumed in imaging remote sensing, L_o is correlated with incoming radiant flux density, E (which is generally from sun and sky), and surface reflectance of object, ρ, by Slater (1980):

$$L_o = \rho\frac{E}{\pi} \quad (10)$$

Beside object radiance, the radiant energy that cames on the detection plane is also contributed by a number of non-target radiance (Figure 2) such as the upward radiance by atmosphere and the glare radiance (flare) which caused by camera system concerned. This is due to the reflection and scattering by the arrangement of lenses, micro inhomogenities in the glass structure, reflection or scattering by mounting equipment, aperture, shutter, and others.

If L_u is upward radiance, τ_u is atmosphere transmittance, and E_f is radiant flux density by the glare, then the radiant flux density formed on the image plane, $E_{i,}$,

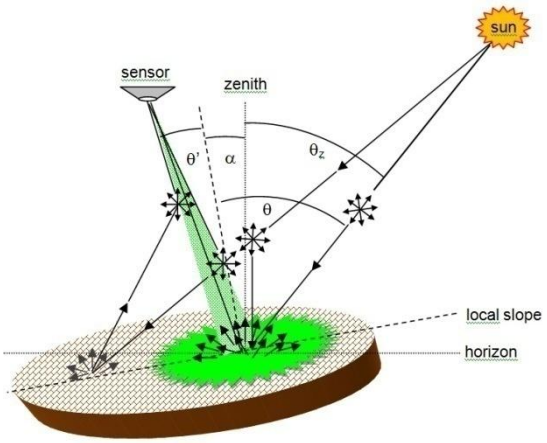

Figure 2. Geometric relation of optical source - object – sensor, and atmosphere crucial role in contributing to non-target radiance in the remote sensing satellite imaging process (modified from Slater, 1980)

can be written as:

$$E_i = \frac{(1-A^2)K_N(\alpha)cos^n\alpha}{4N^2(1-M)^2}[E\rho\tau_u + \pi L_u]\tau_o + E_f \qquad (11)$$

as E in equation (11) is radiant flux density of the sun and sky to the object's surface on earth. E is therefore influenced also by the hour angle or solar zenith angle at which the imaging is done, and it is given by Slater (1980):

$$E = E_0 \cos\theta \exp[-\tau'_{ext}\, sec\, \theta_z] + \pi L_d \qquad (12)$$

with E_0 is radiant flux density on top of atmosphere (t.o.a), θ is the angle between sun and normal line of the object surface (for horizontal flat surface $\theta = \theta_z$), τ'_{ext} is the extinction optical thickness of atmosphere, θ_z is the solar zenith angle, and L_d is downwelling radiance by atmosphere.

First term of the right side of equation (12) is the direct solar radiant flux density. It reaches the Earth's surface at a particular solar zenith angle position. This is shown that the solar zenith angle affects solar irradiance levels in two ways: reducing the radiant flux density as a result of increasing object's surface area caused by increasing solar zenith angle (cosθ factor), and the second is illumination fading because having through the atmosphere with a larger path [τ'_{ext} secθ_z factor].

Many of the quantities in equation (1) to (12) are wavelength dependent. A certain spectrum interval $\Delta\lambda = \lambda_2 - \lambda_1$, total radiant flux density in the image plane E_i, can be calculated by counting the contribution from each part of the wavelength on λ_1 to λ_2 interval or by integrate it in these boundaries.

2.3 Solar Zenith Angle in Imaging Remote Sensing for Equatorial Orbit Satellite

The low earth equatorial orbit satellites, due to its coincide (nearly coincide) of orbital plane to equatorial plane, will pass over a ground track at an extremely wide span of local solar crossing time, from 06.00 local solar time up to 18.00 local solar time. It is corresponding to extremely wide span of hour angle (H), from -90° to +90°. The hour angle is the angular displacement of the sun east or west of the local meridian due to rotation of the earth on its axis at 15° per hour with morning being negative and afternoon being positive. The hour angle is the most decisive variable to the solar zenith angle, and given by Capderou (2005):

$$\cos\theta_z = \sin\phi\sin\delta + \cos\phi\cos\delta\cos H) \qquad (13)$$

where ϕ is latitude position of relevant location, δ is the solar declination angle, and $H = \Lambda - \Lambda_s$ is solar hour angle, with Λ is longitude position of relevant location and Λ_s is the longitude of the sun location at that time. Equation (13) indicates that for the places at zero latitude (the equator) such as Pontianak, Kototabang, and others, on certain dates when the sun is on the equator (March 21 and September 23), solar zenith angle is completely determined by the hour angle at that location.

In one orbit trajectory, maximum earth's arc covered by a satellite (2β) when it seen by an observer P on earth (receiving ground station) is determined by orbital altitude h, and minimum elevation angle required to see the satellite γ (Figure 3). It is given by Capderou (2005):

$$\beta = 2arctan\frac{\sqrt{1+(1/\tan\varsigma)^2 - [R/(R+h)]^2} - (1/\tan\varsigma)}{1+[R/(R+h)]} \qquad (14)$$

where $\varsigma = (90° - \gamma)$ is zenital view angle and R = 6.371×10^6 m is earth radius.

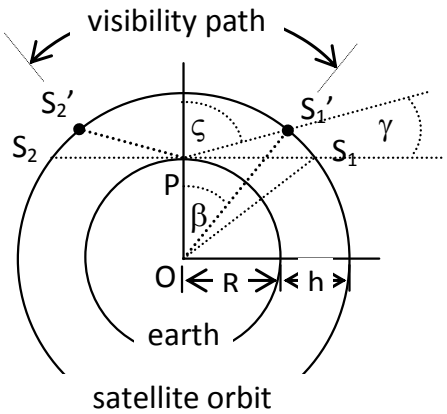

Figure 3. Satellite visibility geometry by observer P on earth (receiving ground station)

For equatorial orbit satellites, this maximum earth's arc covered is equal to the total hour angle difference between start pass and end pass, and it is correspond to visibility time Δt_v, which is given by:

$$\Delta t_v = \frac{\beta}{\pi} T_0(h) \qquad (15)$$

with

$$T_0(h) = \left(1 + \frac{h}{R}\right)^{3/2} x\ 84.4891\ (minutes) \qquad (16)$$

is the satellite orbital period in minutes.

For a low earth equatorial orbit satellite at altitude 650 km, its visibility time from a ground station with γ = 5° is about 11 minutes, which will cover about 40.63° earth longitude, which is equal to nearly 3 different local solar time.

2.4 Pushbroom Imager of LAPAN Satellite

LAPAN pushbroom imager are planned to operate at Vis-NIR region with a spatial resolution in the range of 20 m and three spectral bands. LAPAN pushbroom imager spectral bands proposed to comply with the DMC or Landsat-7 spectral band specification for Vis-NIR region. The three spectral bands are B1(Green): 525-605 nm (Band2 ETM+/LS7), B2(Red): 630-690 nm (Band3 ETM+/LS7), and B3(NIR): 750-900 nm (Band4 ETM+/LS7) (Hasbi *et al.*, 2010).

Optical detector which will be used is single chip tri-linear array type CCD from Kodak, that is Kodak KLI-8023. Each array consists of 8002 detector pixel with a pixel spacing 9 µm and line spacing 108 µm. Under default conditions each array was coated with its own color filter, that is red, green and blue with pass band specifications as shown in Figure 4. Things that quiet interesting from embedded spectral filter of KLI-8023 is transparency in all spectral filter for NIR region (>650 nm). So if KLI-8023 is used without additional external NIR filter the resulting signal from each channel spectrum is a mixture of itself and NIR spectral bands. Implementations of the proposed spectral bands of LAPAN satellite at KLI-8023 thus require modifications to embedded filter that coats the surface of the optical detector elements relevant.

In pushbroom imager, two-dimensional images acquired through shooting objects sequentially line by line with a regular shift sensor system to the object imaged. Therefore, the allocation of the longest exposure time can be provided for the detection device depends on the GSD size and speed of the satellite on the Earth's surface. In order to cover Indonesian territory which lies between latitudes 11° S and 6° N, LAPAN planned to place a satellite on a near equatorial orbit with an inclination less than 10°. While the altitudes not much different from LAPAN micro satellites before, that is around 650 km.

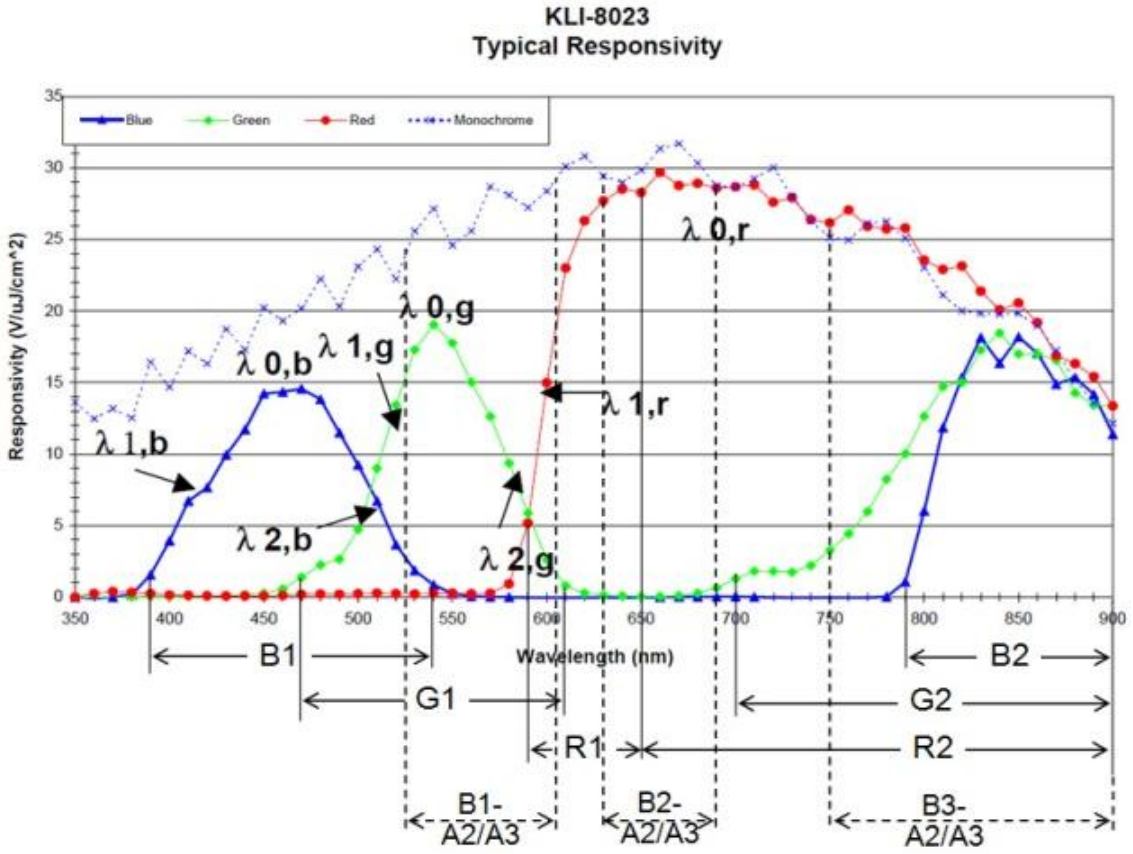

Figure 4. Kodak KLI-8023 detector responsivity that used in LAPAN pushbroom imager and the composition of the selected spectral bands tested in this work. Similar spectrum bands of ETM+/ Landsat-7 which proposed to LAPAN satellite are shown in dashed lines. (Source: Eastman Kodak Company, 2008)

3 MATERIALS AND METHODS

3.1 Estimation of Radiometric Performance for LAPAN Satellite Imager

3.1.1 Approaches and assumptions

LAPAN satellite imager's radiometric performance will be analyzed by using the estimation of voltage generated in cell detector (V_{det}) as a representation of the total radiant energy collected in the image plane due to the incoming radiant energy from the object for a while. V_{det} can be calculated by using equation:

$$V_{det} = E_i t_{int} R_{det} \quad (17)$$

where t_{int} is the integration time or the time of exposure, and R_{det} is the detector responsivity at related passband.

Integration time t_{int} should be calculated from the time needed by the satellite to across a distance of GSD on the earth's surface. The satellite velocity at the earth surface is 6829 m/s due to its height (Hasbi *et al.*, 2010), so that for the 20 meters GSD, t_{int} can be assumed 3 ms. Meanwhile, R_{det} in each pass band is represented by the mean value calculated for full-width band in Figure 4 for each spectral bands selected. Especially for proposed spectrum bands for LAPAN imager, detector responsivity computed from KLI-8023 monochrome responsivity with regard the band pass filter transparency for these bands is 80%.

For simplification, E_i is calculated by equation (11) and (12) just for on axis imaging, regardless such as flare radiance, downwelling radiance, and upwelling radiance, and assume that the optical system used is a full refractive system without a central barrier, so E_i approximated by:

$$E_i = \frac{E_0 \cos\theta_z \exp[-\tau'_{ext} sec\theta_z] \rho \tau_u \tau_o}{4N^2} \quad (18)$$

where $\exp[-\tau'_{ext}\sec\theta_z] = \tau_{\theta z}$ in the right segment of equation (18) is atmospheric transmittance at zenith angle θ_z, and τ_u is $\tau_{\theta z}$ for $\theta_z = 0$.

E_0 in equation (18) calculated from the data of extraterrestrial solar radiant flux density from the American Society for Testing and Materials (ASTM G173-03, Figure 5). Total E_0 for any spectral passband is computed using trapezoidal method. Optical thickness of the atmosphere, τ'_{ext} taken from the Atmospheric Attenuation Model, 1964, Elterman research results released by the Optical Physics Laboratory, Air Force Cambridge Research Laboratories., Lg. Hanscom Field, Mass., USA. Whereas the target reflectance ρ, used grass as the objects in this work, taken from the ASTER Spectral Library Version 2 issued by the California Institute of Technology (Figure 6), while the optical transmittance τ_o is assumed 0.8 for the entire passband selected.

Equation (18) for E_i, and also equation (17) for V_{det} was applied to 3 assumed condition of image sensor, namely KLI-8023 as it is (COTS). This means the selected spectral bands are composed of (390-540 and 790-900) nm for band blue (B), (470-610 and 700-900) nm for band green (G), and (590-650 and 650-900) nm for band red (R). KLI-8023 with additional filter to suppress the incoming NIR radiation (>650nm) installed, which means the selected spectral bands is composed of B1 = (390-540) nm, G1 = (470-610) nm, dan R1 = (590-650) nm. Last, customized KLI-8023 with tailoring embedded filter to 525-605 nm (G), 630-690 nm (R), and 750-900 nm (NIR). Those conditions implemented for imaged targets (green grass, dry grass and conifer), with 3 different values of f-number (N): N = 2.8, N = 4.0, and N = 5.6, and for varying solar zenith angle from 90° to 0° (≈ 06:00 – 12:00 local solar time). The calculated result V_{det} is then converted to digital number DN with saturated output voltage of KLI-8923 (V_{sat} = 5.5 Volt). It is referred as the upper limit value (255). RGB color composite is then created from representative DN as an visual estimation of LAPAN satellite image data.

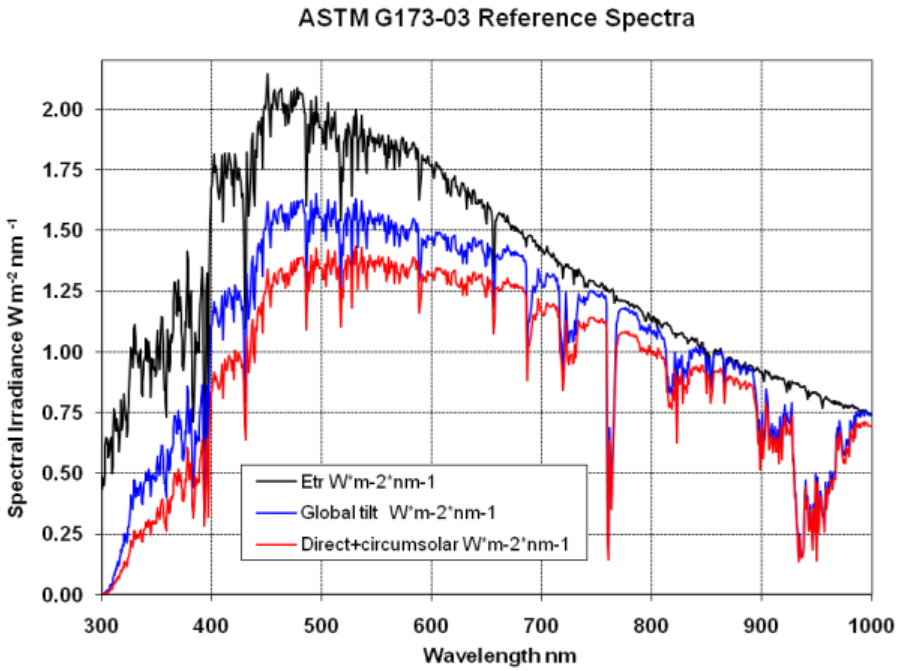

Figure 5. Solar irradiance spectrum (Source: ASTM)

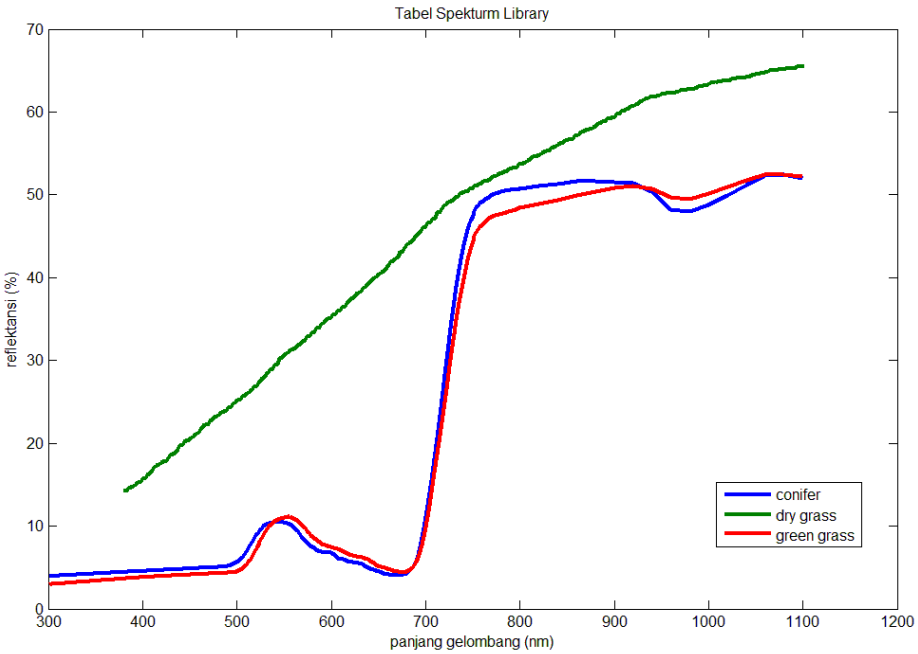

Figure 6. Spectral reflectance of imaged targets (Source: ASTER spectral library version 2)

4 RESULT AND DISCUSSION

4.1 Result

Parameters used in this experiment is summarized as folllows:

- Satellite altitude (h): 650 km
- Inclination (i): < 10°
- Ground velocity (v_g): 6829 m/s
- GSD: 20 m
- Integration time (t_{int}): 3 ms
- Optical transmittance (τ_o): 0.8
- Extinction optical thickness $(\tau'_{ext})_{\lambda=450nm}$: 0.455
- Extinction optical thickness $(\tau'_{ext})_{\lambda=550nm}$: 0.331
- Extinction optical thickness $(\tau'_{ext})_{\lambda=650nm}$: 0.252
- Extinction optical thickness $(\tau'_{ext})_{\lambda=850nm}$: 0.187

Generated Voltage and Estimated RGB Color Composite for Scenario 1 (COTS KLI-8023 without additional filter) Pass Band: B = (390-540 and 790-900) nm, G = (470-610 and 700-900) nm, R = (590-650 and 650-

900) nm are shown in Tabel 2, Figure 7a, and Figure 7b.

Table 2. RESULT VALUES FOR SCENARIO 1

	E_0(W/ m^2nm)	ρ(gg)	ρ(dg)	ρ(cf)	R(V/μJ/ cm^2)
B1	273.92	0.049	0.219	0.058	8.7133
G1	261.96	0.077	0.293	0.077	9.4870
R1	101.21	0.067	0.373	0.058	22.8842
B2	112.67	0.495	0.563	0.513	13.99
G2	228.94	0.438	0.536	0.461	10.17
R2	303.86	0.361	0.515	0.379	24.26

Note: gg=green grasses, dg =dry conifers, cf=conifers

Generated Voltage and Estimated RGB Color Composite for Scenario 2 (COTS KLI-8023 with additional NIR filter to suppress λ > 650 nm installed) Pass Band: B1 = (390-540) nm, G1 = (470-610) nm, R1 = (590-650) nm are shown in Table 3, Figure 8a, and Figure 8b.

Table 3. RESULT VALUES FOR SCENARIO 2

	E_0(W/ m^2nm)	ρ(gg)	ρ(dg)	ρ(cf)	R(V/μJ/ cm^2)
B1	273.08	0.049	0.219	0.058	8.7133
G1	261.32	0.077	0.293	0.077	9.4870
R1	101.21	0.067	0.373	0.058	22.8842

Generated Detector Voltage and Estimated RGB Color Composite for Scenario 3 (embedded color filter of KLI-8023 is tailored to band 2,3,4 of ETM+/LS7) Pass Band: B1(Green) = (525-605) nm, B2(Red) = (630-690) nm, B3(NIR) = (750-900) nm are shown in Table 4, Figure 9a, and Figure 9b.

Table 4. RESULT VALUES FOR SCENARIO 3

	E_0(W/ bm^2nm)	ρ(gg)	ρ(dg)	ρ(cf)	R(V/μJ/ cm^2)
B1	146.123	0.095	0.318	0.088	21.4953
B2	92.733	0.051	0.415	0.046	24.1644
B3	161.631	0.488	0.551	0.509	16.5146

4.2 Discussion

The results of the calculation as presented in Figure 7a, 8a, 9a, 7b, 8b, and 9b, were the representations of LAPAN imager's spectro-radiometric performance if using a Kodak KLI-8023 linear CCD detector for three particular type of imaged targets, the green grass, the dry grass and conifer. These results showed that the use of KLI-8023 as it was (COTS condition) in equatorial orbit provided unsatisfactory radiometric performance, both with additional external filter as recommended by the manufacturer (Figure 8b) and no additional external filter (Figure 7a).

Without the used of additional external filter, for the most wide aperture optic system (N = 2.8), the imager would have over-charged before 9 a.m. It was shown by the value of generated voltage which exceeded the saturated voltage for red spectral band. Similarly, for N = 4.0, the imager could not be operated at time over 10 a.m. Imager could be operated during the daytime when the optical aperture was set at the value of

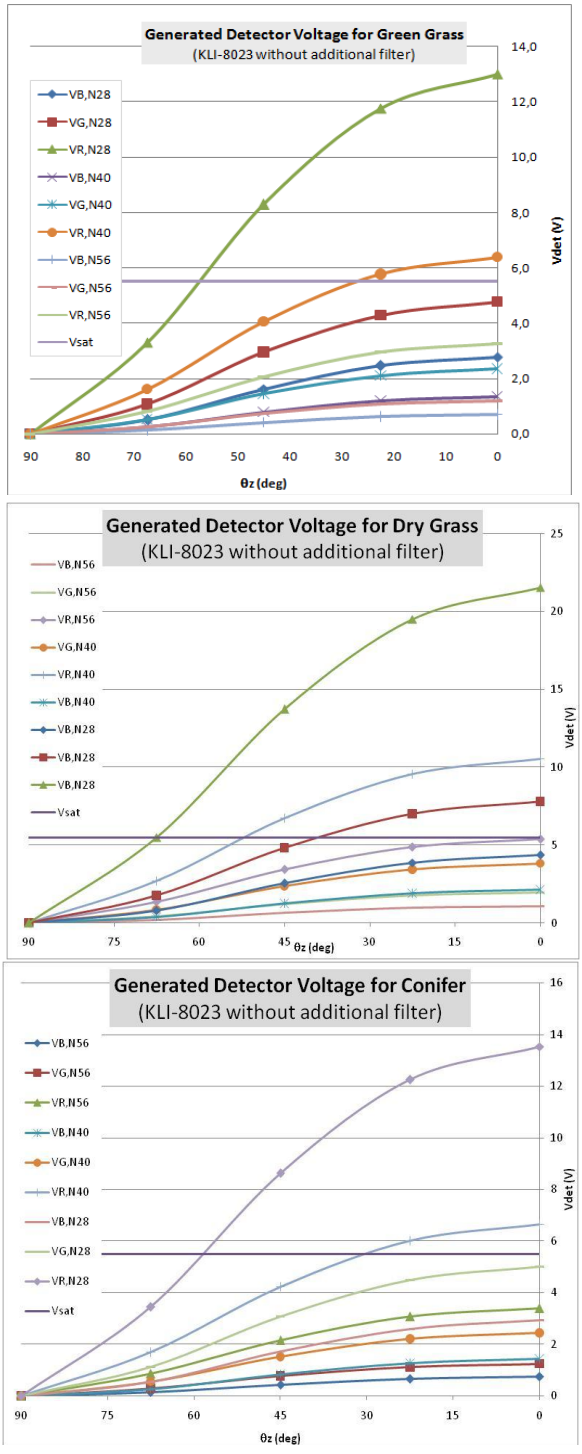

Figure 7a. Generated voltage in Kodak KLI-8023 as a function of solar zenith angle for scenario 1 of selected spectral bands

Green grasses

θ_z (°)	90	67.5	45	22.5	0.0
LST	0600	0730	0900	1030	1200
RGB cc for N=2.8					
RGB cc for N=4.0					
RGB cc for N=5.6					

Dry Grasses

θ_z (°)	90	67.5	45	22.5	0.0
LST	0600	0730	0900	1030	1200
RGB cc for N=2.8					
RGB cc for N=4.0					
RGB cc for N=5.6					

Conifers

θ_z (°)	90	67.5	45	22.5	0.0
LST	0600	0730	0900	1030	1200
RGB cc for N=2.8					
RGB cc for N=4.0					
GB cc for N=5.6					

Figure 7b. Associated RGB color composite (R = VR, G = VG, B = VB) for generated voltage in Figure 7a

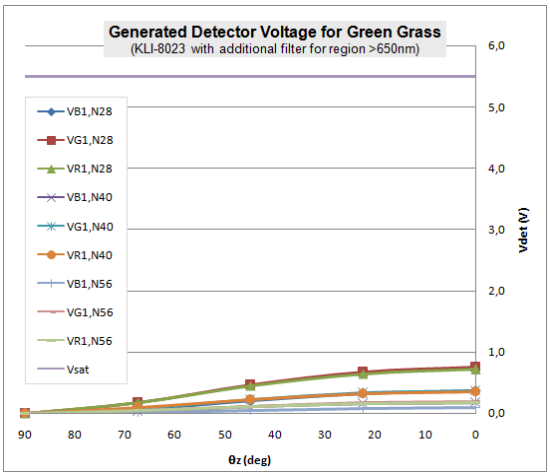

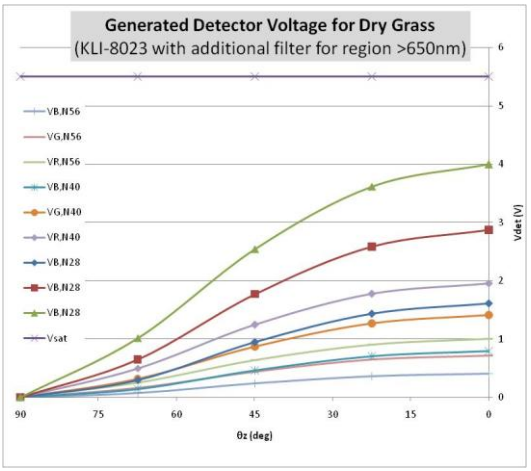

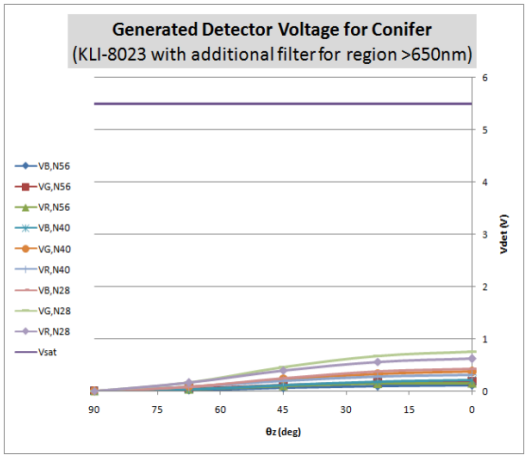

Figure 8a. Generated detector output voltage of Kodak KLI-8023 as a function of solar zenith angle for scenario 2 of selected spectral bands

Green grasses

θ_z (°)	90	67.5	45	22.5	0.0
LST	0600	0730	0900	1030	1200
RGB cc for N=2.8					
RGB cc for N=4.0					
RGB cc for N=5.6					

Dry grasses

θ_z (°)	90	67.5	45	22.5	0.0
LST	0600	0730	0900	1030	1200
RGB cc for N=2.8					
RGB cc for N=4.0					
RGB cc for N=5.6					

Conifers

θ_z (°)	90	67.5	45	22.5	0.0
LST	0600	0730	0900	1030	1200
RGB cc for N=2.8					
RGB cc for N=4.0					
RGB cc for N=5.6					

Figure 8b. Associated RGB color composite (R = VR1, G = VG1, B = VB1) for generated detector voltage in Figure 8a

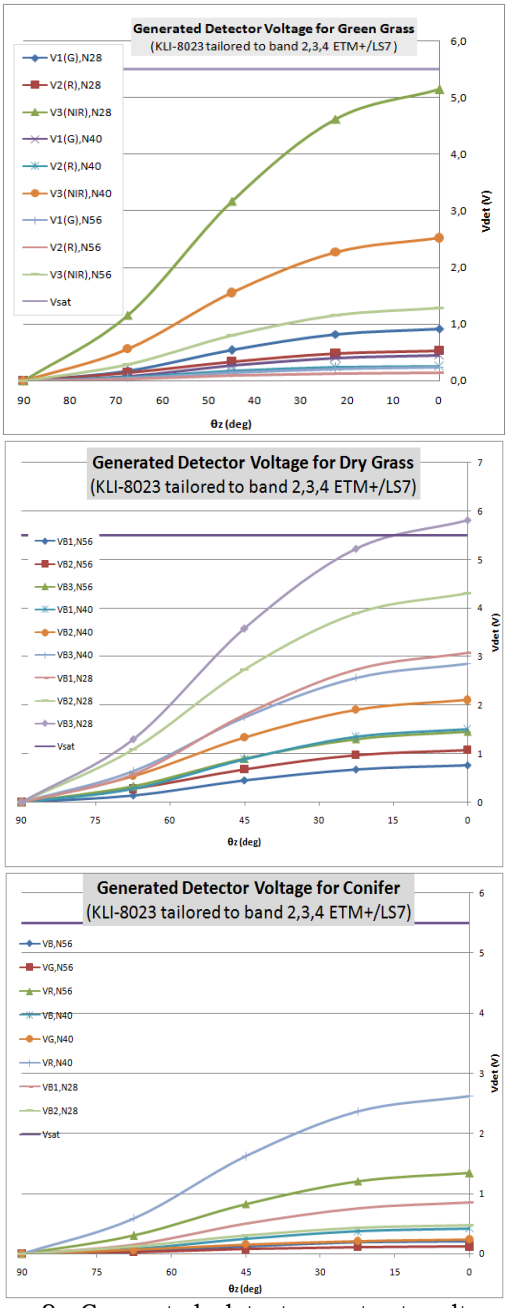

Figure 9a. Generated detector output voltage of Kodak KLI-8023 as a function of solar zenith angle for scenario 3 of selected spectral bands

Green grasses

θ_z (°)	90	67.5	45	22.5	0.0
LST	0600	0730	0900	1030	1200
RGB cc for N=2.8					
RGB cc for N=4.0					
RGB cc for N=5.6					

Dry grasses

θ_z (°)	90	67.5	45	22.5	0.0
LST	0600	0730	0900	1030	1200
RGB cc for N=2.8					
RGB cc for N=4.0					
RGB cc for N=5.6					

Conifers

θ_z (°)	90	67.5	45	22.5	0.0
LST	0600	0730	0900	1030	1200
RGB cc for N=2.8					
RGB cc for N=4.0					
RGB cc for N=5.6					

Figure 9b. Associated RGB color composite (R = V2, G = V3, B = V1) for generated detector voltage in Figure 9a

5.6 or more. For the N value = 5.6, the imager did not experience saturation even in the most sweltering sun condition (θ_z = 0 or ≈ 12 p.m). However, from the composite color simulation for sensors without additional external filter, it appeared that visual imagery was not like the actual color of the imaged target (see Figure 7b).

For additional external filter, which installed to stop the optical radiation above 650 nm, LAPAN imager never had saturated although for most sun condition and wide aperture optic. Unfortunately, for 20 meters GSD in accordance with the 3 ms exposure time, radiant energy accumulated was still very low. The result of voltage calculation

was less than 15% of the highest rate permitted (V_{sat} = 5.5 V, see Figure 8a). Visually, it was shown with the very dark color on the composite color RGB view of the data generated (see Figure 8b). Therefore, the used of additional external filter on KLI-8023 to cut the wavelength above 650 nm, should be compensated with gain to increase the output voltage. In this case, the implementation must also considered the noise gain attached at the detector output. For the 5x gain, estimated composite color RGB of image produced shows a more "accepted" view as shown in Figure 10.

θ_z (°)	90	67.5	45	22.5	0.0
LST	0600	0730	0900	1030	1200
RGB cc for N=2.8					
RGB cc for N=4.0					
RGB cc for N=5.6					

Figure 10. Estimated color composite of imaged target green grass, yielded by LAPAN satellite image sensor using KLI-8023 CCD detector with additional filter to suppress λ > 650nm installed, and Gain = 5x

For customized KLI-8023 which used similar as band 2, 3, 4 of DMC or ETM+/Landsat 7 satellite's imager, the result showed an acceptable spectroradiometric performace of LAPAN imager. Detector had not saturated even though for the most wide optical aperture and the blazing sun (see Figure 9a). However, the combination of customized KLI-8023 with f-number = 2.8 was less recommended due to the possibility of saturation (see voltage values at NIR bands for dry grass at 12 p.m). If the contribution of up-welling radiance, down-welling radiance, and flares have not been counted in the calculation examples above, then it caused an increase in radiant flux density in the image plane by 10%. The used of optical systems with N = 2.8 caused the detector in the NIR bands having saturation when the acquisition time approximately at 12 noon. Therefore, to customized KLI-8023 as Landsat spectrum band, it is advisable to pair it with optical system that is set on aperture or f-number bigger than 2.8 (for example 4.0). RGB color composite simulation for imaged target (green grass), by inputting data from green band on blue channel (B), NIR band on green channel (G), and red band on red channel (R) also gave an impression of a green color. The shades were caused, of course different as those given by the COTS KLI-8023 with NIR filter and Gain 5x (Figure 9b and Figure 10).

5 CONCLUSION

Variation of image radiometric level of a pushbroom imaging system flown on a low earth equatorial orbit satellite was conducted within this work for a sample case with an imaged target green grass at a GSD around 20 meters, Kodak KLI-8023 as the sensor image at 3 spectral bands and 3 optical system aperture (f-number) schemes.

In the selected spectral bands i.e., B = (390-540 and 790-900) nm, G = (470-610 and 700-900) nm, and R = (590-650 and 650-900) nm, imager can be operated throughout the day if f-number 5.6 or greater. For the f-number 4.0 imager having saturation since 10:30 a.m local solar time, while the f-number 2.8 imager has experienced saturation before 9.00 a.m local solar time.

In the modified selected spectral bands, which B = (390-540) nm, G = (470-610) nm, and R = (590-650) nm, the imager can be operated throughout the day without ever experiencing saturation, even very low, for any value of the applied aperture optical systems. On the spectrum bands schemes like this, it is necessary to amplify the output signal.

In the third scenario where the embedded color filters on Kodak KLI-8023 being tailored to bands 2, 3, 4 ETM + / LS-7, which B1 (Green) = (525-605) nm, B2 (Red) = (630-690) nm, and B3 (NIR) = (750-900) nm, the imager can be operated throughout the day on the f-number above 4.0 values without strengthen the output signal.

Estimation of RGB color composite for the two schemes of selected spectral band i.e., scenario 2 and scenario 3 showed a greenish color sense as expected for vegetation imaged target.

REFERENCES

Capderou, M., 2005, Satellites Orbits and Missions, Springer, France.

Eastman Kodak Company, 2005, Kodak kli-8023 image sensor, Revision 4.0 MTD/PS-0219, September 2008.

Elterman, L., 1964, Atmospheric Attenuation Model, 1964, in the

Ultraviolet, Visible, and Infrared Regions for Altitudes to 50 km, Optical Physics Laboratory Project 7670, Air Force Cambridge Research Laboratories, Office Of Aerospace Research, United States Air Force, Lg. Hanscom Field, Mass.

Hasbi, W., M. Mukhayadi, P.A. Budiantoro, A.H. Syafrudin, A.M. Tahir, dan T.M. Kadri, 2010, Penentuan Spesifikasi Optik Kamera Pengamatan Bumi di Satelit LAPAN-A2 dan Satelit LAPAN-A3, Satelit Mikro Untuk Mitigasi Bencana Dan Ketahanan Pangan, IPB Press, ISBN: 978-979-1458-35-1.

Hoeke, A.P. and P.F.J. Linsen, 1984, Workshop Report: Workshop on the A-1 Study of a Joint Indonesian-Netherlands Tropical Earth Resources Satellite (TERS) Program, NIVR-LAPAN, Delft.

Holst, G.C. and T.S. Lomhein, 2007, CMOS/CCD Sensors and Camera Systems, copublished by JCD Publishing and SPIE Press.

Lee, H.C., 2005, Introduction to Color Imaging Science, Cambridge University Press, New York.

Nakamura, J., 2006, Sensors and Signal Processing for Digital Still Cameras, Taylor and Francis, Boca Raton-London - New York – Singapore.

Rudorf, B.F.T., J.C. Epiphanio, Y.E. Shimabukuro, T. Krug, and H.C. Sarvalho, 1996, Applications of the Brazilian Remote Sensing Satellite (SSR) to Monitor the Amazon Region. International Archives of Photo-grametry and Remote Sensing. Vol. XXXI, Part B7, page 599-601. Vienna.

Salatun, J., H. Djojodihardjo, and I. Alisyahbana, 1975, Satellite Orbital Considerations for Remote Sensing in Indonesia, Proceedings, UN-FAO-LAPAN Joint Workshop on Satellite Remote Sensing and Space Communication, Jakarta.

Slater, P.N., 1980, Remote Sensing Optics and Optical Systems, Addison-Wesley Publishing Company, Massachussetts, USA.